Large-scale first principles and tight-binding density functional theory calculations on hydrogen-passivated silicon nanorods

Nicholas Zonias[1]**, Pavlos Lagoudakis**[2] **and Chris-Kriton Skylaris**[1,3]

[1] School of Chemistry, University of Southampton, Highfield, Southampton SO17 1BJ, UK
[2] School of Physics, University of Southampton, Highfield, Southampton SO17 1BJ, UK

E-mail: C.Skylaris@soton.ac.uk

Abstract

We present a computational study by density functional theory (DFT) of entire silicon nanorods with up to 1648 atoms without any periodicity or symmetry imposed. The nanorods have been selected to have varying aspect ratios and levels of surface passivation with hydrogen. The structures of the nanorods have been optimized using a density functional tight-binding approach, while energies and electronic properties have been computed using linear-scaling DFT with plane-wave accuracy with the ONETEP (Skylaris *et al* 2005 *J. Chem. Phys.* **122** 084119) program. The aspect ratio and surface passivation (1×1 and 2×1 reconstructions) along with the size of the nanorods which leads to quantum confinement along all three dimensions, significantly affect their electronic properties. The structures of the nanorods also show interesting behaviour as, depending on their characteristics, they can in certain areas retain the structure of bulk silicon while in other parts significantly deviate from it.

(Some figures in this article are in colour only in the electronic version)

1. Introduction

The applications of silicon nanocrystalline particles have become an extensive and attractive area of research due to their diverse properties. Some of the most important applications involve energy conversion in photovoltaic solar cells [2], biomedical fluorescent imaging as biological sensors [3], and their electrical response in nanoelectronics as field-effect transistors [4, 5], logic circuits [6], light-emitting diodes [7] etc.

The physical and chemical properties of Si nanoparticles can be greatly influenced by their surface chemistry, size and shape. As the size of silicon nanoparticles approaches the quantum regime, their electronic properties are substantially altered compared to a bulk material, due to the strong effect of quantum confinement [8]. Ultrathin silicon nanowires (SiNWs), for instance, demonstrate a blue shift in their

optical spectra [9], while silicon quantum dots (QDs) can emit coloured light depending on their synthetic preparation [10]. Quantum confinement induces photoluminescence in the visible range of silicon particles by increasing their optical gap compared to bulk silicon. Hydrogen-passivated silicon nanoparticles have been a promising material for theoretically investigating the properties of silicon nanostructures, due to their relative simplicity in modelling and for computationally studying them, compared to nanocrystals from other materials.

Various techniques have been developed for experimentally generating hydrogenated silicon nanoparticles. Electrochemical dispersion of bulk silicon followed by ultrasonic fracturing produces oxidized nanocrystalline silicon, which results in a porous layer of one-dimensional crystalline nanowires and zero-dimensional nanocrystals, when treated with hydrofluoric acid (HF) [11]. These nanoclusters are mainly covered by mono-(SiH) and di-(SiH_2) hydride groups and have a very low contamination in SiO_2. Hirata *et al* [12] reported that they were able to obtain completely pure H-passivated silicon

---

[3] Author to whom any correspondence should be addressed.

nanoparticles when oxygen-terminated nanocrystalline silicon films were prepared by using silicon evaporation in an ultra-high vacuum with oxygen and argon radicals and then treated by HF.

Synthesized SiNWs can be growth-controlled, allowing them to be developed not only in different directions but also in various transverse shapes (square, pentagon, hexagon etc) [13]. For restricting the growth to occur along one direction, it is required that the symmetry is broken during growth [14]. The most frequently reported growth directions are the [110], [111], and less frequently, the [112] direction [15]. To our knowledge the thinnest nanowire reported in literature has a diameter of ~1.3 nm [16].

The surface of H-passivated Si nanoparticles determines to a great extent their optical behaviour. There are three surface reconstructions reported in the literature. The (1×1), which contains the highest coverage of hydrogen on the surface atoms, the (2×1), which is formed by the reconstruction of unreconstructed H-passivated Si surfaces to (2×1) monohydride phases and the (3×1) reconstruction [17]. John Northrup [18], using first principles total energy calculations on (2×1), (1×1) and (3×1) H-terminated Si surfaces, showed that at low values of H chemical potential the (2×1) surface reconstruction is more stable, while the (3×1) and (1×1) reconstructions occur when the chemical potential of hydrogen is increased respectively. These conclusions were also confirmed by the computational work of Puzder *et al* [19] who have used quantum Monte Carlo (QMC) and density functional theory (DFT) calculations to study the formation energies of small spherical H-passivated Si nanocrystals.

Depending on the number of atoms that each studied system contains, different computational approaches can be used. In general, tight-binding (TB) methods are used to investigate systems containing from several hundreds to thousands of atoms, DFT methods have been used so far for sizes up to few hundred atoms, combining the time-dependent density functional theory (TDDFT) approach to study excited states and optical spectra [20]. Other methods for studying excited states are based on the self-energy of a many-body GW approach [21] (direct product of a Green Function and a dynamically screened interaction W). Some accurate calculations which have been carried out for small silicon nanoclusters and periodic silicon systems have used quantum Monte Carlo methods [22].

Computational works that are studying silicon nanowires and use DFT methods usually take advantage of the periodicity of a crystalline structure in order to perform calculations about their properties. These works usually employ different techniques for extracting results about electronic properties since DFT within either the generalized gradient approximation (GGA) or local density approximation (LDA) [23] underestimates band gaps, in some cases even by a factor of two [8]. Despite this, DFT can predict reliably the geometries and the band structure when varying the diameter or the surface of these nanoclusters.

In this work we present a DFT study of silicon nanorods with more than 1000 atoms. In order to perform DFT calculations on such a large scale we do not take advantage

of periodicity or symmetry (as in nanowires), but we perform calculations directly on the entire nanorods by using the ONETEP program for linear-scaling DFT with plane-wave accuracy [1].

Details about the linear-scaling method developed in the ONETEP program, are given in section 2. In sections 2.1 and 2.2 we describe the procedure we have followed to study the nanocrystals and some validation tests we have performed to confirm the reliability of the parameters used in our calculations. In section 3, we present our results and discuss them in the context of other works from the literature. Finally our conclusions are summarized in section 4.

2. Theoretical approach

The DFT calculations were performed within the GGA method using the Perdew, Burke and Ernzerhof (PBE) exchange–correlation functional [24]. For the *ab initio* DFT calculations, the ONETEP [1] software package was used, while for the tight-binding DFT calculations, we used the DFTB+ code [25].

ONETEP [1] is a linear-scaling approach for DFT calculations, which is based on the reformulation of DFT in terms of the one-particle density matrix. In terms of Kohn–Sham orbitals, the density matrix is represented as

$$\rho(\mathbf{r}, \mathbf{r}') = \sum_{n=0}^{\infty} f_n \psi_n(\mathbf{r}) \psi_n^*(\mathbf{r}'), \tag{1}$$

where $\psi_n(\mathbf{r})$ is a Kohn–Sham orbital and f_n is its occupancy.

An equivalent representation is

$$\rho(\mathbf{r}, \mathbf{r}') = \sum_{\alpha\beta} \phi_\alpha(\mathbf{r}) K^{\alpha\beta} \phi_\beta^*(\mathbf{r}'), \tag{2}$$

where $\phi_\alpha(\mathbf{r})$ are localized non-orthogonal functions [26] and $K^{\alpha\beta}$, which is called the density kernel, is the representation of f_n in the duals of these functions. Most commonly in linear-scaling approaches the density kernel is optimized while keeping $\phi_\alpha(\mathbf{r})$ in some suitable form (e.g. pseudoatomic orbitals). Linear scaling is achieved by truncating the density kernel, thus exploiting the exponential decay of the density matrix (in non-metallic systems [27]). A particular characteristic of ONETEP is that the localized functions $\phi_\alpha(\mathbf{r})$ are also optimized during the calculation, subject to a localization constraint, and are thus known as non-orthogonal generalized Wannier functions (NGWFs [28]). The NGWFs are expanded in a basis set of periodic sinc (psinc) functions [29], which are equivalent to a plane-wave basis as they are related by a unitary transformation. The fact that NGWFs are optimized *in situ* allows plane-wave accuracy to be achieved with only a minimal number of NGWFs (and hence the smallest possible sparse matrices); furthermore, the psinc basis is independent of atomic positions and provides a uniform description of space; ONETEP calculations are not affected by basis set superposition error [30]. The code is parallelized and allows calculations to be performed on large systems containing thousands of atoms [31, 32].

DFTB+ [25] is a density functional tight-binding code which exploits the sparsity of the TB equations and uses conventional dense diagonalization algorithms to construct the density matrix for delivering a reliable and efficient implementation. The matrix size increases linearly with the number of atoms, for large systems, while all the matrices are real for both periodic and non-periodic systems. The method developed in the code is based on the second-order expansion of the Kohn–Sham DFT energy with respect to charge density fluctuations [33]. A generic expression for the total self-consistence charge (SCC) DFTB energy is given by

$$E_{\text{DFTB}} = \sum_n^{\text{occ}} \langle \psi_n | \hat{H}_0 | \psi_n \rangle + \frac{1}{2} \sum_{\alpha,\beta}^N \gamma_{\alpha\beta} \Delta q_\alpha \Delta q_\beta. \quad (3)$$

The first term runs over the occupied single-particle wavefunctions ψ_n and calculates the Hamiltonian energy for an input density n_0, which is equivalent to a common standard non-self-consistent TB scheme. The second term represents the second-order extension of the Kohn–Sham energy of wavefunctions and potentials centred on atoms α and β. The charge fluctuations Δq_α and Δq_β of atoms α and β are defined by a SCC redistribution of Mulliken charges. $\gamma_{\alpha\beta}$ consists of a long-range pure Coulomb term and an exponentially decaying short-range function S:

$$\gamma_{\alpha\beta} = \frac{1}{R_{\alpha\beta}} - S(R_{\alpha\beta}, U_\alpha, U_\beta), \quad (4)$$

where $R_{\alpha\beta}$ is the distance between atoms α and β, and U_α and U_β are the Hubbard parameters for these atoms respectively.

2.1. Methodology

The H-terminated silicon nanorods were constructed with Accelrys Materials Studio[4]. The [111] growth direction has been chosen to be the preferential elongation axis, since this is the mainly observed growth direction in several experimental works [15]. All the constructed nanorods have a fixed length of 5.0 nm with diameters varying from 0.8 nm to 1.3 nm. The nanostructures were carefully shaped in order to avoid the existence of SiH_3 on the surface when saturating the dangling bonds of silicon atoms with hydrogen, as these groups are highly reactive [15]. Thus, the surface of the (1×1) unreconstructed H-passivated Si nanorods contained both dihydrides (SiH_2) and monohydrides (SiH), while the (2×1) reconstruction surface contained only monohydrides to allow a uniform distribution of reconstructed units. The nanorods were placed in a periodic box with a minimum 1 nm vacuum region to eliminate periodic interactions.

The nanorods were then pre-optimized, using tight-binding DFT, within a 0.05 eV Å^{-1} force tolerance. The pre-optimization is required to distinguish the preferred tendencies for reconstruction, mainly for the (2×1) nanostructures. Any single dangling bonds that remained after the pre-optimization on the surface Si atoms were capped with hydrogens.

A full geometry optimization was then carried out with DFTB+ [25] for all the nanoclusters, and afterwards, the

---

[4] Accelrys *Materials Studio* Inc Accelrys Software, ©2001–2007.

Table 1. Comparison of Si–Si and Si–Si bond lengths as calculated with CASTEP [34], NWCHEM [35], ONETEP [1] and DFTB+ [25] for $Si_{29}H_{36}$.

Interaction	Interatomic distances (Å)			
	ONETEP	CASTEP	NWCHEM	DFTB+
Si–Si[a]	2.326	2.335	2.343	2.363
Si–Si[a]	2.319	2.325	2.337	2.339
Si–H[a]	1.503	1.487	1.509	1.503
Si–H[a]	1.498	1.480	1.503	1.498

[a] Si–Si neighbour distances of inner shell.
[b] Si–Si neighbour distances of outer shell.
[c] Si–H distances of Si atoms containing a single H.
[d] Si–H distances of Si atoms containing two H.

coordinates of the optimized structures were imported into the ONETEP code, to perform DFT energy and electronic properties calculations, using a psinc kinetic energy cut-off of 300 eV. 6 NGWFs with 7.0 Å radius, for each Si atom, and 1 NGWF with 6.0 Å radius, for each H atom, were found to be sufficient for the representation of Si and H atoms in the calculation, after several tests on smaller systems, which are summarized in the next section.

2.2. Validation tests

For choosing suitable parameters for our ONETEP calculations several tests on the small $Si_{29}H_{36}$ quantum dot and the $Si_{242}H_{140}$ nanoplate model clusters have performed using a variety of approaches.

In the case of $Si_{29}H_{36}$, DFT geometry optimizations, using the PBE exchange–correlation functional, were performed with ONETEP [1], CASTEP [34] (plane-wave DFT), NWCHEM [35] (Gaussian basis set DFT) and DFTB+ [25] (tight-binding DFT). An energy tolerance of 0.2 meV per atom and a force tolerance of 0.05 eV Å^{-1} were used as convergence criteria for CASTEP, ONETEP and DFTB+. For the NWCHEM calculations, the 6-31+G* basis set was used to describe both Si and H atoms.

As can be observed from the results summarized in table 1 the optimized structures have the central atom in a tetrahedral coordination, which approaches almost identically the symmetry of a Si atom in bulk silicon, while the surface interatomic distances of neighbour silicon atoms are slightly shorter than the core. Similar geometries were obtained by Sundholm [36] in his simulations on $Si_{29}H_{36}$, using DFT and coupled-cluster methods.

It is worth noting the remarkable agreement between the Si–H bond lengths described by ONETEP and DFTB+, even though the two programs use different approximation methods but still the same exchange–correlation functional. On the other hand, the Si–Si neighbour distances as calculated with ONETEP tend to agree better with the distances calculated by CASTEP. Both programs are *ab initio* DFT codes which use plane waves to describe the electronic wavefunction in contrast with NWCHEM which uses Gaussian basis sets.

Previously, calculations on crystalline silicon with ONETEP obtained the best results when 9 NGWFs are used

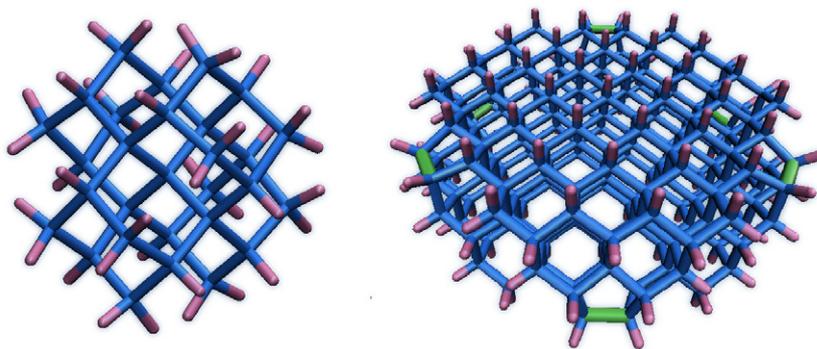**Figure 1.** ONETEP optimized structures of $Si_{29}H_{36}$ and $Si_{242}H_{140}$.

Figure 2. Schematic representation of symmetric hydrogens (before geometry optimization) and 'canted' hydrogens (after geometry optimization) located on a part of the surface of the (1×1) reconstructed $Si_{766}H_{462}$ nanorod.

for representing the Si atoms [37]. However, we found that by reducing the NGWFs from 9 to 6 and the kinetic energy cut-off from 650 to 300 eV, the final geometries of $Si_{29}H_{36}$ change only slightly ($\sim$1% in bond lengths and angles) and are still acceptable, as these errors are less than those due to the other approximations involved in DFT calculations.

The band gap of $Si_{29}H_{36}$, using ONETEP within the local density approximation (LDA) for the optimized structure, was 3.75 eV, in good agreement with the LDA band gap calculated by Puzder *et al* [38] (3.6 eV) and with the band gap reported by Wang *et al* [39] (3.67 eV). When the B3LYP [40] exchange–correlation functional is used, the ONETEP calculation yields a 5.3 eV band gap, which is in excellent agreement with QMC results from reference [38] (5.3 eV) and B3LYP/6-31G(d) calculations from reference [39] (5.32 eV). Unfortunately the current implementation of B3LYP in ONETEP is not linear scaling and does not allow us to study systems much larger than $Si_{29}H_{36}$. The experimental excitation threshold of 3.5 eV [41] given to a hydrogenated Si_{29} nanoparticle mainly refers to the $Si_{29}H_{24}$ [42–44].

For testing the geometry optimization effectiveness in achieving surface reconstructions, sample calculations with ONETEP and DFTB+ using a slice from a 2.0 nm thick nanorod ($Si_{242}H_{140}$) have been performed. The structure was constructed with 12 free dangling bonds on the surface Si atoms, to allow 6 reconstructions to happen. After several geometry steps, the 6 reconstructions did occur. With ONETEP, the calculations were performed using a force tolerance of 0.05 eV Å^{-1} and a kinetic energy cut-off of 650 eV. In contrast with $Si_{29}H_{36}$ tests, in which an effectively infinite value for the kernel cut-off distance was used, in this case, the spatial cut-off of the density kernel was set to 13.23 Å. The optimized structure is shown in figure 1, were the reconstructed Si–Si bonds have been highlighted. The DFTB+
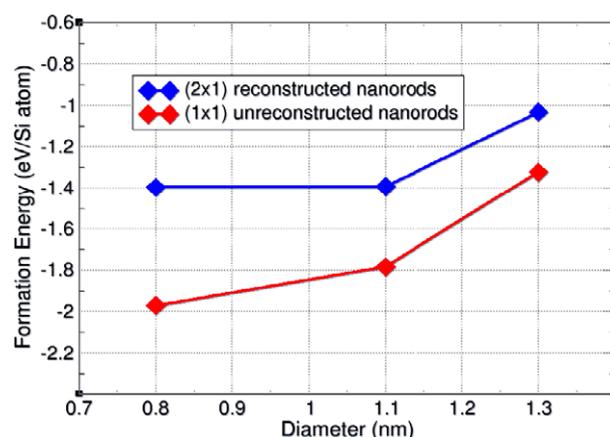

Figure 3. Formation energies of the (2×1) reconstructed (blue) and (1×1) unreconstructed (red) nanorods.

optimized structure is in close agreement with the ONETEP, similar to $Si_{29}H_{36}$.

3. Results and discussion

3.1. Structural properties

Each diagram of figure 4 shows two kinds of distribution; the distribution of nearest neighbour interatomic distances between silicon atoms along the caps of the nanorod and the distribution along the main part. As expected, due to the different shape between the caps and the main body of the nanorod, the deformation of interatomic distances creates a bigger dispersion of points, which becomes more apparent in the thinnest (2×1) nanostructure, and as the diameter increases the fitting curves between the caps and the main part tend
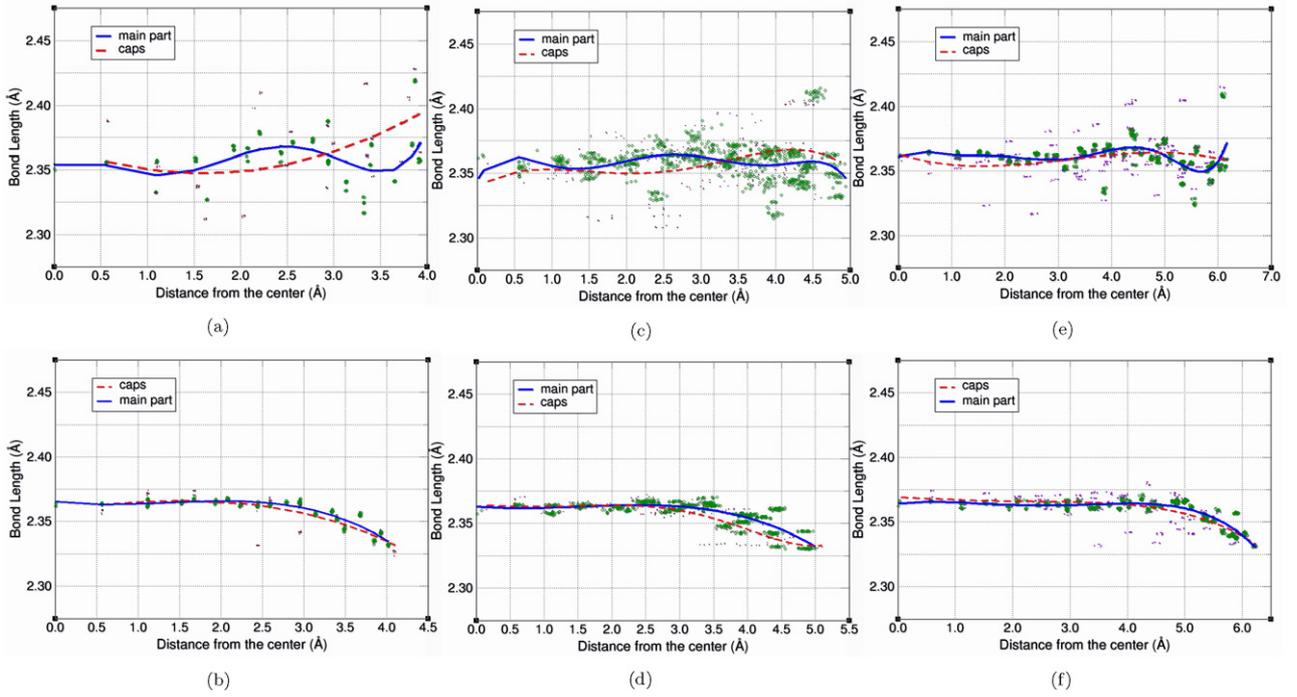
Figure 4. Diagrams of nearest neighbour interatomic distances in $Si_{532}H_{224}$ (a), $Si_{532}H_{308}$ (b), $Si_{766}H_{318}$ (c), $Si_{766}H_{402}$ (d), $Si_{1186}H_{366}$ (e), $Si_{1186}H_{462}$ (f). Si–Si bond lengths located at the caps are represented with dots while bond lengths located in the main part are shown with circles.

to coincide. As can be observed, there is a homogeneous distribution of the Si–Si distances from the centre of mass, 'core', which is later disrupted as we reach the surface. Si–Si bond lengths located at the inner part are distributed around 2.36 Å, which is the Si–Si distance in bulk silicon calculated using the PBE exchange–correlation functional, for all the H-passivated silicon nanostructures. Approximately 25% of the total volume for the thinnest nanorod maintains the structural properties of the bulk crystal and as the diameter of the nanorod increases this can extend up to 45% for the (2×1) reconstructed nanorods, while for the (1×1) unreconstructed nanorods this range goes approximately from 60% to 75%.

Moving along the diameter of the nanorod from the core to the surface, structural differences between the reconstructed (2×1) and unreconstructed (1×1) nanostructures emerge. Si–Si neighbour distances of the (2×1) reconstructed nanorods present a non-uniform behaviour across the whole volume, having a range between 2.33 and 2.42 Å. The (1×1) reconstructed surfaces present a similar dispersion of Si–Si interatomic distances for all the studied diameters, in which the bond length becomes significantly shorter ($\sim$2.33 Å) while the points of the inner part are equally dispersed around the fitting curve in all the (1×1) nanorods. This tendency, is also observed in several theoretical studies on H-passivated silicon nanowires [15, 45] and can be justified by the steric hindrance the hydrogen atoms exert on the silicon atoms of the surface. The Si–H interatomic distances are distributed around 1.50 Å, which are in agreement with the results obtained by Nolan *et al* [45] (1.53 Å), who have performed DFT calculations with the PBE exchange–correlation functional on silicon nanowires with diameters of about 1 nm. Despite

that, they have found that a 'canted' conformation between surface hydrogen atoms does not occur in (1×1) reconstructed surfaces, while our results show that the 'canted' conformation can actually occur in specific parts of the surface, as proposed also by Vo *et al* [15]. Schematic representations of 'canted' hydrogens observed in our structures are shown in figure 2.

Furthermore, the diagrams clearly show a grouping of points on specific areas of interatomic distances as we move from the centre to the surface of each nanorod, mainly at the main part (away from the caps). This is another factor in support of structural stability and a homogeneous dispersion along the length of the nanorod. Although this pattern applies in the majority of the studied nanostructures, the difference observed, mainly in the $Si_{766}H_{318}$ nanorod (diagram (c) of figure 4), results from the presence of both dimers (SiH_2) and monomers (SiH) on the surface.

3.2. Electronic properties

In order to investigate the electronic properties of the (1×1) unreconstructed $Si_{532}H_{308}$, $Si_{766}H_{402}$, $Si_{1186}H_{462}$ and (2×1) reconstructed $Si_{532}H_{224}$, $Si_{766}H_{318}$, $Si_{1186}H_{366}$ nanorods and the influence by their surfaces and aspect ratios, DFT calculations using ONETEP, on the TB optimized structures have been performed.

The stabilities of the nanorods were determined by calculating their formation energies (E_f) using the formula [46]:

$$E_f = \frac{(E^{tot} - (n_H E_H))}{n_{Si}} - E_{Si}, \qquad (5)$$

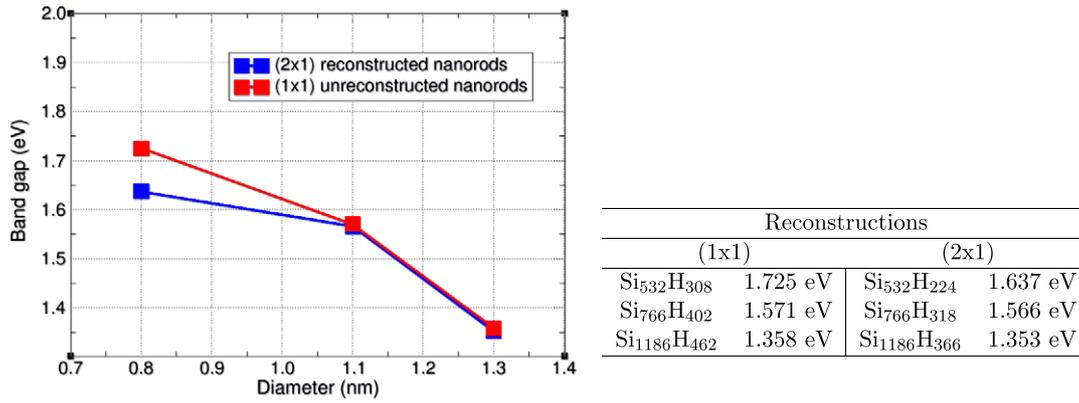| Reconstructions			
(1x1)		(2x1)	
$Si_{532}H_{308}$	1.725 eV	$Si_{532}H_{224}$	1.637 eV
$Si_{766}H_{402}$	1.571 eV	$Si_{766}H_{318}$	1.566 eV
$Si_{1186}H_{462}$	1.358 eV	$Si_{1186}H_{366}$	1.353 eV

Figure 5. Energy band gaps of optimized H-terminated Si structures calculated with ONETEP [1] using the PBE exchange correlation functional [24].
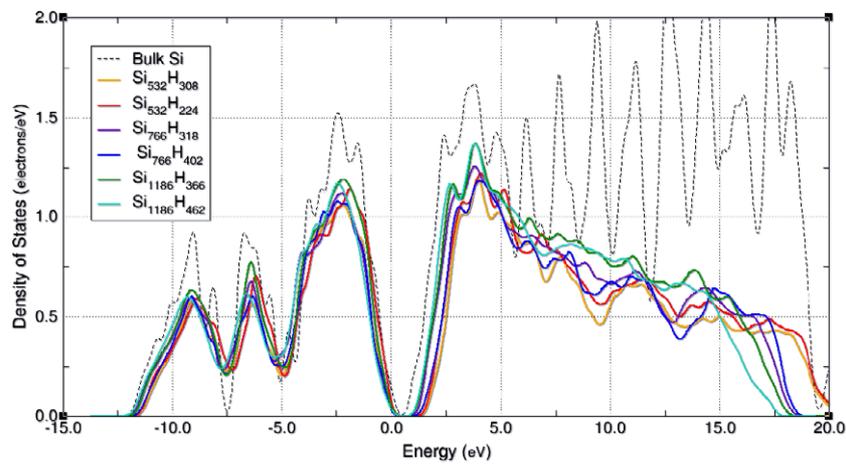

Figure 6. Density of states (DOS) of $Si_{532}H_{308}$, $Si_{766}H_{402}$, $Si_{1186}H_{462}$, $Si_{532}H_{224}$, $Si_{766}H_{316}$ and $Si_{1186}H_{366}$ as calculated with ONETEP [1]. The DOS for bulk silicon (dotted line) has been calculated with CASTEP [34]. In both programs the PBE exchange–correlation functional was used.

where E^{tot} is the total energy of the Si nanorod, n_{Si} and n_H are the number of silicon and hydrogen atoms contained in it, E_{Si} is the energy of one Si atom in a bulk silicon crystal and E_H the energy H atom in a H_2 molecule. For calculating the energies E_{Si} and E_H single point energy calculations were performed with ONETEP for bulk silicon and for a H_2 molecule.

The results plotted in figure 3 confirm at first, the stability of the studied nanoclusters, with formation energies lying between -2.0 to -1.0 eV per Si atom. The (1×1) unreconstructed nanorods with the highest coverage in hydrogen, have lower formation energies compared to the (2×1) reconstructed nanorods. Secondly, figure 3 reveals that as the number of atoms increases the stabilities decrease and as the size of our nanoclusters approaches the bulk limit, they are expected to become zero. The stabilities of the $Si_{532}H_{224}$ and the $Si_{766}H_{316}$ nanorods appear very similar and this can be justified by the presence of dihydride (SiH_2) groups on the (2×1) reconstructed surface of the $Si_{766}H_{316}$, which induce less strain between the reconstructed surface parts and consequently lower the formation energy.

An important feature related to the optical properties of silicon nanostructures is their band gap. It has been observed that the energy band gaps of silicon nanostructures can be affected by their diameter, surface structure and the growth direction, in the case of silicon nanowires. As the diameter of a nanostructure is decreased the energy band gap increases, due to quantum confinement effects [8]. This phenomenon is observed in the majority of the silicon structures studied at the nanoscale such as quantum dots [19], nanowires [47] or nanotubes [48]. In the case of silicon nanowires, this trend also applies not only on structures with different growth directions but also between nanowires with different surface reconstructions [49].

The values reported in the table of figure 5 represent the HOMO–LUMO gap obtained directly from GGA-DFT calculations using the PBE exchange–correlation functional. Although it is known that GGA methods generally underestimate energy band gaps they can still provide qualitative trends of optical gaps. A self-energy correction method, such as the GW approach, has not been attempted due to the prohibitive amount of computer time such a calculation would require in its application to our nanoclusters.

Our calculations show a reduction of the band gap as the diameter of the nanorod is increased. Although this work is on non-periodic hydrogenated silicon nanorods, our band gaps appear to follow trends similar to works on periodic
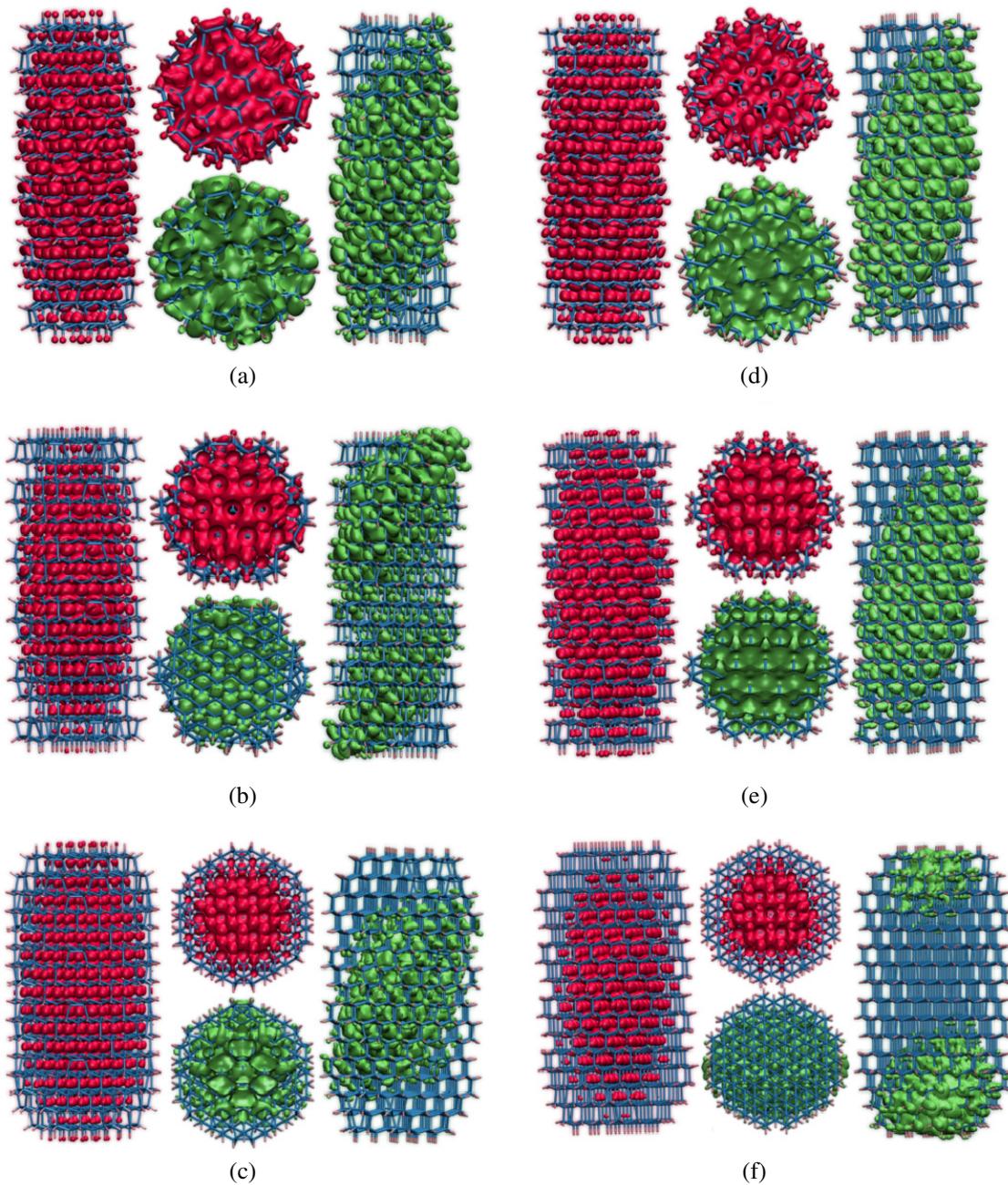
(a)

(d)

(b)

(e)

(c)

(f)

Figure 7. Representations of HOMO (red—left and top) and LUMO (green—right and bottom) orbital density plots for $Si_{532}H_{224}$ (a), $Si_{532}H_{308}$ (d), $Si_{766}H_{318}$ (b), $Si_{766}H_{402}$ (e), $Si_{1186}H_{366}$ (c), $Si_{1186}H_{462}$ (f) nanorods. Each diagram shows a horizontal view from each orbital, parallel to the nanorod's growth axis, and a vertical view, by clipping the nanorod through a plane at its centre of mass. The isosurfaces were generated by using an isovalue of $1 \times 10^{-5} \frac{e}{a_0^3}$.

H-terminated silicon nanowires. For instance, Vo *et al* [15] reported that both the (1×1) and (2×1) reconstructed surfaces of [111] grown silicon nanowires reduce their band gaps from 2.12 eV to 0.85 eV and from 1.54 eV to 0.84 eV respectively, as their diameter increases from 1.1 to 3.0 nm, by performing first principles calculations. Zhao *et al* [8], using the LDA approach including GW corrections [50], found that the band gap of [111] Si nanowires also decreases from 2.3 to 0.8 eV as their thickness increases from 0.9 to 3.2 nm. In a similar work by Saita *et al* [51], the energy band gaps of [111] Si nanowires with diameters 0.55 to 1.0 nm varied from 2.83 to 1.90 eV.

Figure 5 also shows that the reconstructed surfaces tend to have smaller band gaps from the unreconstructed. Although this trend is obvious in the nanorods with diameters 0.8 nm the coincidence of the lines between the reconstructed and unreconstructed surfaces for the 1.1 nm and the 1.3 nm thick nanorods indicates the small role played by the surface as the diameter of the nanorods increases.

The reduction of the band gap can also be observed in figure 6. The plots show the total electronic density of states (DOS) of the nanoclusters $Si_{532}H_{308}$, $Si_{766}H_{402}$, $Si_{1186}H_{462}$,

$Si_{532}H_{224}$, $Si_{766}H_{318}$ and $Si_{1186}H_{366}$ and of bulk crystalline silicon. While the DOS peaks placed in the valence band area are in close agreement between the nanorods and the bulk silicon, there is strong disagreement for the conduction bands. This phenomenon was also observed in the work of Skylaris and Haynes [37] who performed DFT calculations within the LDA scheme on a 1000-atom silicon lattice and concluded that the ONETEP NGWFs are usually only capable of describing correctly the valence and the low-lying conduction bands. The DOS of the nanorods in the valence area for the (1×1) reconstructed surfaces follow closely the DOS of bulk silicon. This also justifies the use of H-passivated silicon nanoclusters for drawing conclusions regarding the properties of pure silicon nanostructures.

The ability of the ONETEP code to perform DFT calculations directly on nanostructures containing thousands of atoms allows us also to obtain the molecular orbitals for entire nanostructures. Isosurfaces of the HOMO and LUMO orbital densities of the studied hydrogenated silicon nanorods are given in figure 7.

The HOMO orbitals of all the nanostructures and the LUMO orbitals of $Si_{532}H_{224}$, $Si_{532}H_{308}$, $Si_{766}H_{402}$ and $Si_{1186}H_{366}$ are localized at the centre of mass. The LUMO orbitals are degenerate, and in all the studied nanorods they intersect the growth axis at an angle. Surprisingly the LUMO orbitals of the $Si_{766}H_{402}$ and the $Si_{1186}H_{462}$ show a localization closer to the caps of the nanorod, with the LUMO orbital of $Si_{1186}H_{462}$ localized exclusively at the caps. A quite similar phenomenon was observed in the LUMO orbitals of reconstructed and unreconstructed quantum dots with 0.8 nm diameter [19], although in this case the localization of the orbital is shifted from the core to the surface when going from an unreconstructed (1×1) to a reconstructed (2×1) surface. As the hydrogen passivation of the surface provides a relatively small barrier for electrons and holes, the HOMO and LUMO orbitals spill out more from the core as the diameter is reduced.

While computational studies on silicon nanowires have shown the dependence of the band gap on the growth direction, diameter and surface reconstruction, our results show that these factors also strongly affect the electronic properties of H-passivated nanorods, despite the fundamental differences between finite, short nanorods and infinite length nanowires. The shift in the localization of the HOMO and LUMO densities, from the core to the surface for the LUMO, while the HOMO remains in the core, can be compared to the transformation of the energy band gap from 'direct' to 'indirect'.

4. Conclusions

We have presented a computational study by DFT of silicon nanorods with varying aspect ratios and surface passivation by hydrogen, without use of symmetry or periodicity (as in the case of nanowires). The DFT calculations were performed on the entire structures with more than 1000 atoms by using the ONETEP linear-scaling DFT program. This approach has allowed us to examine the structural, energetic and electronic properties of the nanorods at the atomistic *ab initio* level of detail.

Our calculations revealed that the inner part of the nanorod retains a structure close to bulk Si, while approaching the surface this stability is distorted. In the (1×1) unreconstructed nanorods Si–Si bond lengths become more condensed, while in the (2×1) reconstructed nanorods the range of the Si–Si bond length distribution becomes wider and larger as we move from the 'core' to the surface. Furthermore, the (1×1) surfaces adopt the 'canted' conformation between neighbour H atoms, which is consistent with several theoretical studies reported previously.

The (1×1) unreconstructed H-passivated nanorods have higher stabilities compared to the (2×1) reconstructed nanostructures, which tend to decrease as the diameter of the nanorod is increased. According to our calculations, when the diameter of the nanorod is extended by 5 Å, formation energies per Si atom decay almost by 1 eV. Similarly, a reduction of $\sim$0.5 eV for the (1×1) nanorods and of $\sim$0.3 eV for the (2×1) nanorods in the HOMO–LUMO band gap is observed when their diameter is increased from 8–13 Å.

References

[1] Skylaris C-K, Haynes P D, Mostofi A A and Payne M C 2005 Introducing ONETEP: linear-scaling density functional simulations on parallel computers *J. Chem. Phys.* **122** 084119
[2] Stupca M, Alsalhi M, Al Saud T, Almuhanna A and Nayfeh M H 2007 Enhancement of polycrystalline silicon solar cells using ultrathin films of silicon nanoparticle *Appl. Phys. Lett.* **91** 063107
[3] Cui Y, Wei Q, Park H and Lieber C M 2001 Nanowire nanosensors for highly sensitive and selective detection of biological and chemical species *Science* **293** 1289–92
[4] Cui Y and Lieber C M 2001 Functional nanoscale electronic devices assembled using silicon nanowire building blocks *Science* **291** 851–3
[5] Koo S-M, Li Q, Edelstein M D, Richter C A and Vogel E M 2005 Enhanced channel modulation in dual-gated silicon nanowire transistors *Nano Lett.* **5** 2519–23
[6] Huang M H, Mao S, Feick H, Yan H, Wu Y, Kind H, Weber E, Russo R and Yang P 2001 Room-temperature ultraviolet nanowire nanolasers *Science* **292** 1897–9
[7] Huang Y, Duan X, Cui Y, Lauhon L J, Kim K-H and Lieber C M 2001 Logic gates and computation from assembled nanowire building blocks *Science* **294** 1313–7
[8] Zhao X, Wei C M, Yang L and Chou M Y 2004 Quantum confinement and electronic properties of silicon nanowires *Phys. Rev. Lett.* **92** 236805
[9] Canham L T 1990 Silicon quantum wire array fabrication by electrochemical and chemical dissolution of wafers *Appl. Phys. Lett.* **57** 1046–8

[10] Erogbogbo F, Yong K-T, Roy I, Xu G, Prasad P N and Swihart M T 2008 Biocompatible luminescent silicon quantum dots for imaging of cancer cells *ACS Nano* **2** 873–8

[11] Xie Y H, Wilson W L, Ross F M, Mucha J A, Fitzgerald E A, Macaulay J M and Harris T D 1992 Luminescence and structural study of porous silicon films *J. Appl. Phys.* **71** 2403–7

[12] Hirata M, Nakamura K and Yokota K 2005 H-termination of nanocrystalline Si:O films by HF solution treatment *e-J. Surf. Sci. Nanotechnol.* **3** 527–30

[13] Yao D, Zhang G and Li B 2008 A universal expression of band gap for silicon nanowires of different cross-section geometries *Nano Lett.* **8** 4557–61

[14] Lieber C M 1998 One-dimensional nanostructures: chemistry, physics & applications *Solid State Commun.* **107** 607

[15] Vo T, Williamson A J and Galli G 2006 First principles simulations of the structural and electronic properties of silicon nanowires *Phys. Rev.* B **74** 045116

[16] Ma D D D, Lee C S, Au F C K, Tong S Y and Lee S T 2003 Small-diameter silicon nanowire surfaces *Science* **299** 1874–7

[17] Chabal Y J and Raghavachari K 1985 New ordered structure for the H-saturated Si(100) surface: the (3×1) phase *Phys. Rev. Lett.* **54** 1055–8

[18] Northrup J E 1991 Structure of Si(100)H: dependence on the H chemical potential *Phys. Rev.* B **44** 1419–22

[19] Puzder A, Williamson A J, Reboredo F A and Galli G 2003 Structural stability and optical properties of nanomaterials with reconstructed surfaces *Phys. Rev. Lett.* **91** 157405

[20] Zdetsis A D, Garoufalis C S, Skaperda M S and Koukaras E N 2005 Variation and adjustment of the optical gap of small Si nanocrystals by partial substitution of Si with Ge *J. Phys.: Conf. Ser.* **10** 101–4

[21] Hybertsen M S and Louie S G 1985 First-principles theory of quasiparticles: calculation of band gaps in semiconductors and insulators *Phys. Rev. Lett.* **55** 1418–21

[22] Puzder A, Williamson A, Grossman J and Galli G 2002 Surface control of optical properties in silicon nanoclusters *J. Chem. Phys.* **117** 6721–9

[23] Jensen F 1999 *Introduction to Computational Chemistry* (New York: Wiley)

[24] Perdew J P, Burke K and Ernzerhof M 1996 Generalized gradient approximation made simple *Phys. Rev. Lett.* **77** 3865–8

[25] Aradi B, Hourahine B and Frauenheim Th 2007 DFTB+, a sparse matrix-based implementation of the DFTB method *J. Phys. Chem.* A **111** 5678–84

[26] Hernández E, Gillan M J and Goringe C M 1996 Linear-scaling density-functional-theory technique: the density-matrix approach *Phys. Rev.* B **53** 7147–57

[27] Kohn W 1996 Density functional and density matrix method scaling linearly with the number of atoms *Phys. Rev. Lett.* **76** 3168–71

[28] Skylaris C-K, Mostofi A A, Haynes P D, Diéguez O and Payne M C 2002 Nonorthogonal generalized Wannier function pseudopotential plane-wave method *Phys. Rev.* B **66** 035119

[29] Mostofi A A, Haynes P D, Skylaris C-K and Payne M C 2003 Preconditioned iterative minimization for linear-scaling electronic structure calculations *J. Chem. Phys.* **119** 8842–8

[30] Haynes P D, Skylaris C-K, Mostofi A A and Payne M C 2006 Elimination of basis set superposition error in linear-scaling density-functional calculations with local orbitals optimised *in situ Chem. Phys. Lett.* **422** 345–9

[31] Skylaris C-K, Haynes P D, Mostofi A A and Payne M C 2006 Implementation of linear-scaling plane wave density functional theory on parallel computers *Phys. Status Solidi* b **243** 973–88

[32] Skylaris C-K, Haynes P D, Mostofi A A and Payne M C 2008 Recent progress in linear-scaling density functional calculations with plane waves and pseudopotentials: the ONETEP code *J. Phys.: Condens. Matter* **20** 064209

[33] Elstner M, Porezag D, Jungnickel G, Elsner J, Haugk M, Frauenheim Th, Suhai S and Seifert G 1998 Self-consistent-charge density-functional tight-binding method for simulations of complex materials properties *Phys. Rev.* B **58** 7260–8

[34] Segall M D, Probert M J, Pickard C J, Hasnip P J, Clark S J, Payne M C and Refson K 2005 First principles methods using CASTEP *Z. Kristallogr.* **220** 567–70

[35] Bylaska E J, de Jong W A, Govind N, Kowalski K, Straatsma T P, Valiev M, Wang D, Apra E, Windus T L, Hammond J, Nichols P, Hirata S, Hackler M T, Zhao Y, Fan P-D, Harrison R J, Dupuis M, Smith D M A, Nieplocha J, Tipparaju V, Krishnan M, Wu Q, Van voorhis T, Auer A A, Nooijen M, Brown E, Cisneros G, Fann G I, Fruchtl H, Garza J, Hirao K, Kendall R, Nichols J A, Tsemekhman K, Wolinski K, Anchell J, Bernholdt D, Borowski P, Clark T, Clerc D, Dachsel H, Deegan M, Dyall K, Elwood D, Glendening E, Gutowski M, Hess A, Jaffe J, Johnson B, Ju J, Kobayashi R, Kutteh R, Lin Z, Littlefield R, Long X, Meng B, Nakajima T, Niu S, Pollack L, Rosing M, Sandrone G, Stave M, Taylor H, Thomas G, Van lenthe J, Wong A and Zhang Z 2007 *NWChem, A Computational Chemistry Package for Parallel Computers* Pacific Northwest National Laboratory

[36] Sundholm D 2003 First principles calculations of the absorption spectrum of $Si_{29}H_{36}$ *Nano Lett.* **3** 847–9

[37] Skylaris C-K and Haynes P D 2007 Achieving plane wave accuracy in linear-scaling density functional theory applied to periodic systems: a case study on crystalline silicon *J. Chem. Phys.* **127** 164712

[38] Puzder A, Williamson A J, Grossman J C and Galli G 2003 Computational studies of the optical emission of silicon nanocrystals *J. Am. Chem. Soc.* **125** 2786–91

[39] Wang B C, Chou Y M, Deng J P and Dung Y T 2008 Structural and optical properties of passivated silicon nanoclusters with different shapes: a theoretical investigation *J. Phys. Chem.* A **112** 6351–7

[40] Becke A D 1993 Density-functional thermochemistry. III. The role of exact exchange *J. Chem. Phys.* **98** 5648–52

[41] Nayfeh M H, Rigakis N and Yamani Z 1997 Photoexcitation of Si-Si surface states in nanocrystallites *Phys. Rev.* B **56** 2079–84

[42] Mitas L, Therrien J, Twesten R, Belomoin G and Nayfeh M H 2001 Effect of surface reconstruction on the structural prototypes of ultrasmall ultrabright Si_{29} nanoparticles *Appl. Phys. Lett.* **78** 1918–20

[43] Draeger E W, Grossman J C, Williamson A J and Galli G 2003 Influence of synthesis conditions on the structural and optical properties of passivated silicon nanoclusters *Phys. Rev. Lett.* **90** 167402

[44] Lehtonen O and Sundholm D 2006 Coupled-cluster studies of the electronic excitation spectra of silanes *J. Chem. Phys.* **125** 144314

[45] Nolan M, O'Callaghan S, Fagas G, Greer J C and Frauenheim Th 2007 Silicon nanowire band gap modification *Nano Lett.* **7** 34–8

[46] Chan T L, Ciobanu C V, Chuang F C, Lu N, Wang C Z and
Ho K-M 2006 Magic structures of H-Passivated ⟨110⟩
silicon nanowires *Nano Lett.* **6** 277–81

[47] Singh A K, Kumar V, Note R and Kawazoe Y 2006 Effects of
morphology and doping on the electronic and structural
properties of hydrogenated silicon nanowires *Nano Lett.*
6 920–5

[48] Ming N, Guangfu L, Jing L, Lin L, Lu W, Mingwei J, Wei S,
Zhengxiang G, Guangping L, Wang N M and
Dapeng Y 2007 First-principles study of
hydrogen-passivated single-crystalline silicon nanotubes:
electronic and optical properties *Nanotechnology* **18** 505707

[49] Ng M-F, Zhou L, Yang S W, Sim L Y, Tan V B C and
Wu P 2007 Theoretical investigation of silicon nanowires:
methodology, geometry, surface modification, and electrical
conductivity using a multiscale approach *Phys. Rev.* B
76 155435

[50] Hybertsen M S and Louie S G 1986 Electron correlation in
semiconductors and insulators: band gaps and quasiparticle
energies *Phys. Rev.* B **34** 5390–413

[51] Saitta A M, Buda F, Fiumara G and Giaquinta P V 1996 *Ab
initio* molecular-dynamics study of electronic and optical
properties of silicon quantum wires: orientational effects
Phys. Rev. B **53** 1446–51